Partha P. Shome, Taimoor Khan, Binod K. Kanaujia, Ahmed A. Kishk, and Yahia M. M. Antar

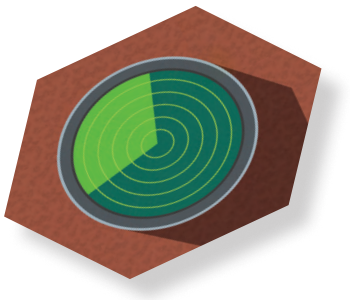

Unidirective Miniaturized Ultrawideband Antenna for Sensing Buried Objects in Handheld Ground-Penetrating Radar Systems

A design approach.

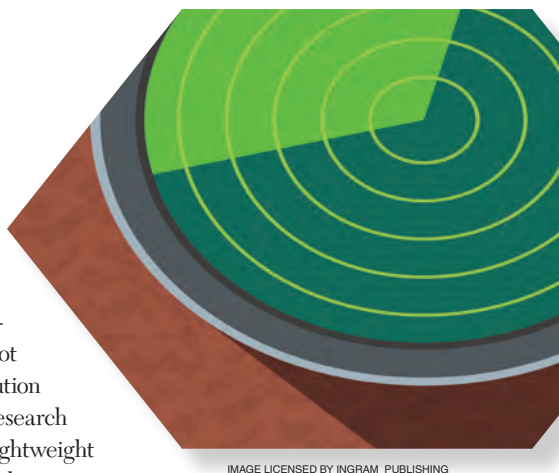

IMAGE LICENSED BY INGRAM PUBLISHING

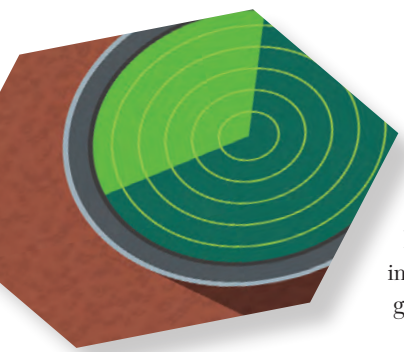

Ground-penetrating radars (GPR) using ultrawideband (UWB) technology have attracted a lot of research interests worldwide for high-resolution sensing and material characterization. This research contribution, therefore, introduces a miniaturized lightweight UWB antenna with high-gain characteristics for applications in handheld GPR systems. The high-gain antenna is developed to function in the 3.13–11.74-GHz wide frequency range such that it can allow high-resolution sensing of buried targets, such as landmines, metal pipes, and other structures. An elliptical quadrant-shaped UWB monopole radiator with a protuberant ground plane is conceptualized to constitute a highly miniaturized antenna of size 18×11 mm^2. The standalone UWB antenna realizes an impedance bandwidth of 3.07–11.67 GHz with a peak gain of 2.9 dBi. Next, a single-side copper-coated dielectric substrate as a reflector is placed beneath the antenna to attain a significant gain improvement. The proposed design with a reflector provides an average gain improvement of about 7.1 dB without influencing the original bandwidth. For experimental validation, a prototype is fabricated and characterized. The measured performance reveals close agreement with the simulation with an operating

Digital Object Identifier 10.1109/MAP.2022.3203311
Date of current version: 10 November 2022

bandwidth of 3.19–11.83 GHz and a maximum gain of approximately 10 dBi at 4.02 GHz.

INTRODUCTION

The research interests in UWB technology have led to the innovation of multiple wireless applications enabling high-speed and reliable data communication. GPR is one such major application that is extensively used to sense and localize buried objects for military and civilian applications. GPR technology is also applied to other applications, such as archaeological studies, geophysical research, road-quality assessment, fault detection, and others [1]. In all of these applications, the target location usually ranges from a few centimeters to several meters. The number of applications is further increasing with the inception of newly developed detection techniques and algorithms. The working mechanism of GPR systems involves a nondestructive testing technique that utilizes an electromagnetic (EM) signal to sense buried objects. Figure 1 represents the typical functional block diagram of a GPR system. The GPR technology has the potential of locating and identifying both metallic and nonmetallic objects. The fundamental requirements of a GPR system include high penetration capability with good range resolution. Today, lightweight handheld GPR systems are also in demand for easy transportation [2].

A distinctive and essential component of the GPR system is the antenna. To realize a sufficient resolution range (in centimeters) for detecting miniaturized object details, antennas should have a wide operational bandwidth [3]. Therefore, a UWB antenna, by virtue of its wide bandwidth characteristics, helps in achieving high-resolution imaging. Typical UWB antennas applied for GPR cover broad bandwidths from megahertz to gigahertz. In general, a low frequency of operation is used to sense deeply buried objects as high-frequency signals undergo high energy attenuation within the propagating media [4]. Different UWB antenna types, such as the loaded dipole [5], horn antenna [6], and Vivaldi antenna [7], are introduced to operate typically in a frequency span of megahertz. However, these classes of antennas introduce mobility constraints because of their bulky configurations and thus fail to satisfy the demand for actual field-portable applications. On the other hand, the radiation at frequencies above 1 GHz usually achieves a higher resolution of the targeted objects despite a reduced penetration depth. Now, the penetration capacity of transmitted signals can be enhanced significantly by employing high-gain UWB GPR antennas [8].

Taking into account the mobility constraints, printed UWB antennas, like tapered-slot antennas [9], [10], bow-tie antennas [11], and monopole antennas [12], are now widely developed for portable GPR devices. However, achieving high-gain characteristics with printed UWB antennas remains an interesting research topic. The antenna gain is expected to be improved further by redirecting the undesired back radiation to the desired main beam direction. Placing a reflector plane below the antenna ground plane could be a solution [13], [14]. Different reflector types, like solid metal cavities [2] or dielectric material [16], can be used. Lately, artificial magnetic conductors (AMCs) [17] and frequency-selective surfaces (FSSs) [18], [19], [20], [21] have also been introduced to amplify the gain in UWB antennas. However, a solid metallic cavity reflector seems heavy, which becomes a concerning factor for practical implementations.

Similarly, designing AMC and FSS structures with ultrawide operating characteristics imposes multiple challenges because of their electrical complexity and fabrication sensitivity. Besides, the AMC-based design introduced in [17] has an unstable gain variation throughout the UWB operating bandwidth. The FSS reflectors introduced in [18] and [19] make the overall system too bulky and complicated. The dual-layer FSS used in [20] also possesses a high design complexity with a poor gain enhancement of approximately 4 dB across the antenna operating bandwidth.

Given the mentioned limitations, authors have experimented with developing a printed UWB quasi-monopole antenna with high-gain and broadside directive radiation characteristics to meet the GPR system requirements. A rectangular one-side copper-coated dielectric material has been utilized as a reflecting material below the ground plane for gain-enhancement purposes. An in-depth performance analysis of the UWB antenna and the effect of the reflector plane on bandwidth, gain, and radiation characteristics are analyzed in depth. The novelty of the proposed work can be summarized as the realization of 1) a highly miniaturized configuration of a quasi-monopole antenna for UWB application, without any significant degradation in the different antenna performance parameters, like bandwidth, gain, and radiation characteristics; a 2) a cost-effective and simple approach for gain enhancement in UWB antennas by the placement of a copper-coated dielectric reflector; and 3)

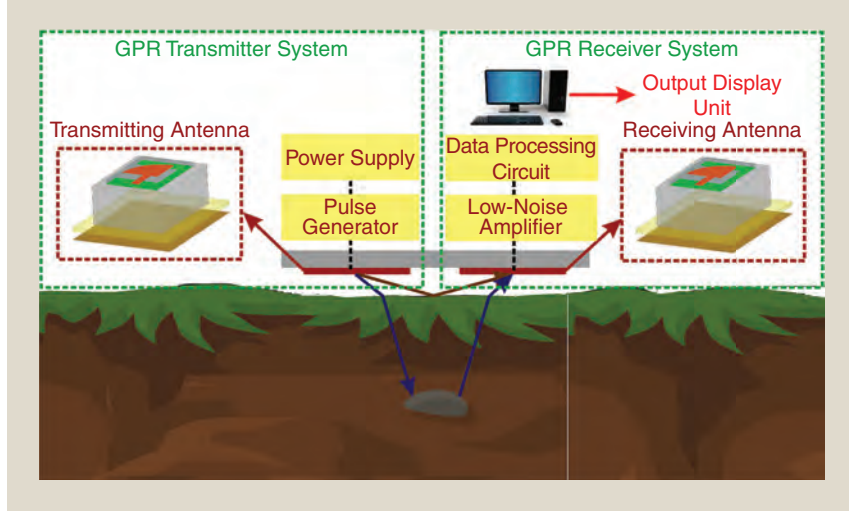

FIGURE 1. A GPR system for underground object identification.

a theoretical study to predict the amplitude and phase of the reflected power from the proposed planar reflector.

The proposed work realizes a lightweight and miniaturized GPR antenna system for conveniently identifying hidden objects in portable handheld GPR systems. The design and performance analysis of the reflector-backed UWB antenna has been done using the full-wave 3D simulator Ansys High-Frequency Structure Simulator v16 [22]. In this article, the section "Antenna Geometry Description" introduces the antenna geometry. The theory of the reflector plane in gain enhancement is studied mathematically and included in the section "Theory of Reflector Plane in Gain Enhancement." The section "Simulation Analysis" illustrates the parametrical study of the reflector-backed antenna, whereas the experimental characterization of the proposed work is presented in the section "Fabrication and Experimental Validation." The final section presents the concluding remarks of this investigation process.

ANTENNA GEOMETRY DESCRIPTION

This section introduces the geometrical descriptions of the individual monopole UWB antenna and the antenna backed by the reflector. The UWB monopole is printed on a low-cost FR4 substrate with relative permittivity $\varepsilon_r = 4.4$, loss tangent $\tan\delta = 0.02$, and thickness $h = 0.8$ mm.

UWB ANTENNA DESIGN

The proposed UWB antenna geometry is introduced in Figure 2(a). An elliptical quadrant-shaped radiator fed by a 50-Ω microstrip line is printed on the top side of the FR4 dielectric substrate. On the bottom side, a ground plane, backing the microstrip line and extended to form a C-shape, surrounds the monopole radiator from three sides. The C-shaped ground plane helps in realizing wide impedance matching and miniaturization of the antenna. The final optimized dimensions (in millimeters) of the proposed UWB antenna are obtained as $X_S = 11$, $Y_S = 18$, $Y_1 = 2.5$, $Y_2 = 5.6$, $X_1 = 7.36$, $X_2 = 8.28$, $X_3 = 2.7$, $X_4 = 3.5$, and $X_f = 1.8$. UWB characteristics using such a highly miniaturized configuration and without any significant degradation of the antenna performance parameters, including bandwidth, gain, and radiation characteristics, have not been achieved in the existing literature. To highlight the percentage of miniaturization realized by the proposed antenna, a comparison with the recent literature is carried out for size and performance characteristics, as shown in Table 1. A minimum 45% reduction in size is achieved compared to [24], and a maximum 96% reduction is noticed with reference to [29]. In addition to achieving miniaturization, the proposed antenna design also maintains a suitable performance matrix within its usable bandwidth.

UWB ANTENNA WITH REFLECTOR

Figure 2(b) displays the geometrical sketch of the top side of the UWB monopole, and its relative position with respect to the reflector of a dielectric slab backed by metal is shown in Figure 2(c). The dielectric slab with metalized back is an FR4 material placed at $S = 18$ mm parallel to the antenna plane. The reflector position is selected to redirect the back radiation toward the broadside to enhance the antenna gain. The optimization of the reflector dimensions reaches $X_R \times Y_R = 41 \times 48$ mm^2. The design parameters associated with the reflector structure are obtained as $h_r = h_g = h_{rs} = 0.035$ mm and $h_{r1} = 0.8$ mm. The thickness of the reflector substrate is selected considering different factors, like the creation of surface waves, weight constraints, material cost, and its physical role.

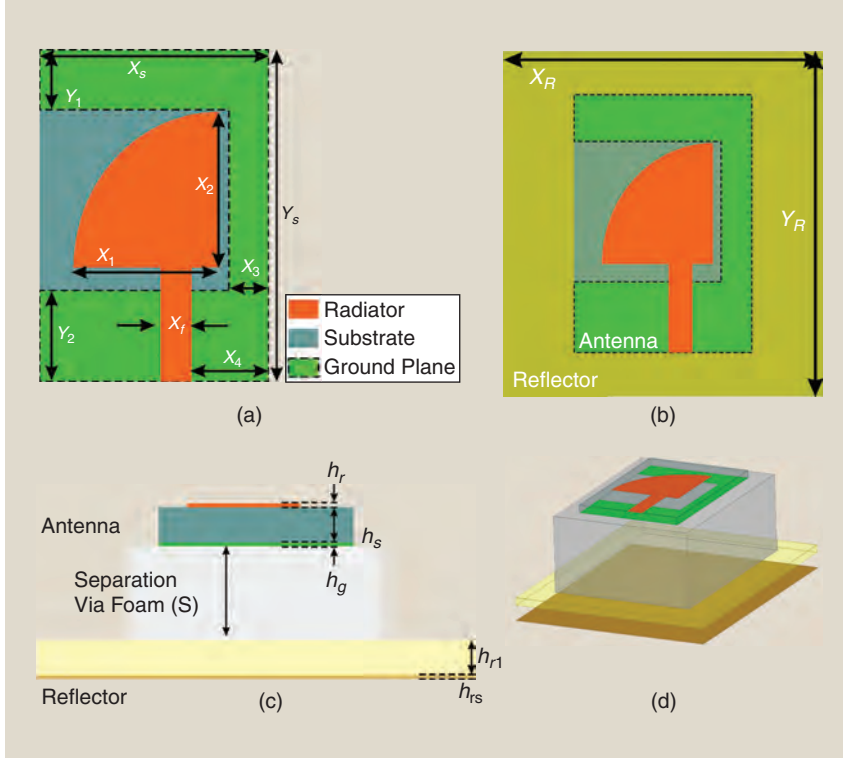

FIGURE 2. A schematic diagram of the proposed UWB GPR antenna. (a) Top view, (b) top view backed by a reflector, (c) cross-sectional view, and (d) 3D view.

THEORY OF REFLECTOR PLANE IN GAIN ENHANCEMENT

In this section, an analytical approach to assess the effect of the proposed reflector in enhancing the overall system gain is described. It is expected that the gain will improve significantly by redirecting the back radiation and allowing it to add to the main beam, constructively [30]. Usually, conductor reflectors are placed at a quarter wavelength from the antenna to enhance the gain by 3 dB over a narrow band. However, we require the reflector to

enhance the gain over a wide band. Thus, the reflector is loaded with the dielectric slab, and its parameters (dimensions and location) are utilized to maximize the gain enhancement. The working mechanism is depicted in Figure 3(a). The reflected waves should be almost in phase with the forwarding waves, such that their superposition results in a high gain in the broadside direction over a wide band. Next, to assess the reflectance and transmittance capacity of the reflector, the reflection coefficient of the system is derived theoretically using transmission line theory. The different regions of the proposed reflector system, shown in Figure 2(c), are perceived as a section of the transmission line, as displayed in Figure 3(b). For approximation and simplification of the results, we assume that the plane wave is generated at the antenna position and a distance S from the dielectric interface, which is a substrate of thickness h_{r1}. The other dielectric side is depicted as a load that can be shorted with a conductor or left as air.

Now, the total input impedance (Z_{in}) looking from the source can be obtained as [31]

$$Z_{in} = \eta_0 \frac{Z_{1,2} + j\eta_0 \tan(\beta_0 S)}{\eta_0 + jZ_{1,2}\tan(\beta_0 S)}, \quad (1)$$

where η_0, $\beta_0 = \omega/c$, S, and $Z_{1,2}$ are the intrinsic impedance of the free space, the phase constant in the free space, the air medium height (in meters), and the input impedance looking from the air–reflector interface, respectively.

$$Z_{1,2} = \eta_S \frac{Z_{2,3} + j\eta_S \tan(\beta_S h_{r1})}{\eta_S + jZ_{2,3}\tan(\beta_S h_{r1})}, \quad (2)$$

$$Z_{2,3} = \begin{cases} 0, \text{ with conductor termination} \\ \eta_0, \text{ with free space termination}' \end{cases} \quad (3)$$

where $\eta_S = \eta_0\sqrt{\mu_r/\varepsilon_r}$, $\beta_S = \beta_0\sqrt{\mu_r\varepsilon_r}$, h_{r1}, and $Z_{2,3}$ are the intrinsic impedance of the dielectric medium, the phase constant in the dielectric medium, the thickness of the dielectric medium (in meters), and the input impedance looking from the reflector–load interface, respectively.

Finally, using (1)–(3), the ratio of reflected to incident power can be calculated as

$$\frac{P_{ref}}{P_{in}} = |\Gamma|^2 = \left|\frac{Z_{in} - \eta_0}{Z_{in} + \eta_0}\right|^2. \quad (4)$$

By substituting the values of Z_{in} and η_0 in (4), the ratio of the reflected power (P_{ref}) to the incident power (P_{in}) is obtained as ~1, when the dielectric reflector is left with conductor termination. This represents that an almost complete amount of the input power is sent back by the reflector. Similarly, for free space

TABLE 1. UWB ANTENNA PERFORMANCE COMPARISON WITH EXISTING DESIGNS.

Reference	Dimensions (mm × mm × mm) and Volume (mm^3)	Impedance Bandwidth (GHz)	Peak Gain (dBi)	Radiation Efficiency	Substrate Permittivity
[23]	25 × 14.1 × 1.6 (= 564)	2.2–11	~ 6	N.A.	4.4
[24]	34 × 14.7 × 0.787 (= –394)	2.4–11	N.A.	N.A.	2.2
[25]	20 × 10 × 1.4 (= 280)	3.1–12	N.A.	N.A.	4.4
[26]	19 × 12 × 1.6 (= 364.8)	2.95–12	3.18	~ 80 %	4.4
[27]	20 × 26 × 1.52 (= 790.4)	3.1–11.8	3.86	N.A.	2.17
[28]	20 × 16 × 1.6 (= 512)	3.25–13	~ 4.5	N.A.	N.A.
[23]	28.4 × 28.15 × 1.6 (= 1,280)	3.3–12.1	N.A.	N.A.	N.A.
[29]	90.5 × 60.1 × 0.813 (= 4,422)	3.1–11	~ 9	N.A.	3.55
This work	**18 × 11 × 0.8 (= 158.4)**	**3.07–11.67**	**~ 3.4**	**~ 80 %**	**4.4**

N.A.: not available.

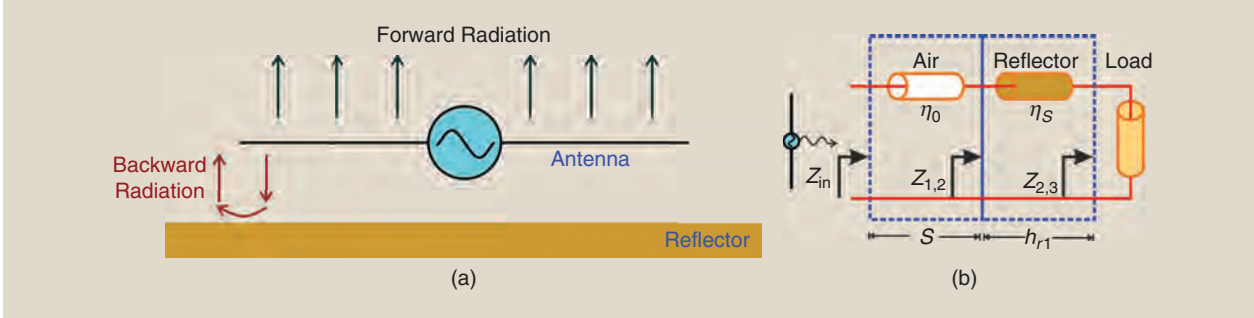

FIGURE 3. (a) The radiation mechanism of a reflector-backed antenna. (b) The transmission line analogy of the proposed multilayer wave propagation.

termination, the ratio of P_{ref} to P_{in} can be computed as ~ 0.20, representing a 20% reflection of the backward traveling wave. Based on this study, it can be inferred that a dielectric with conductor termination can be considered a preferable alternative for gain enhancement. Additionally, the phase of the reflected signal is also required to be in coherence with the forwarding waves for constructive interference. The following equation is used to obtain the phase (ϕ_T) at the plane of the antenna:

$$\phi_T = \phi_R + \phi_S, \tag{5}$$

where ϕ_R and ϕ_S are the phases at the reflector plane and the round-trip free space propagation delay between the antenna and the reference plane. Also,

$$\phi_S = 2 \times \frac{\omega}{c} S. \tag{6}$$

For phase coherence, ϕ_T should be zero or an integral multiple of 2π within the operating bandwidth. Figure 4 shows that the predicted reflection phase at the antenna plane, obtained using (5), is consistent and close to the desired phase value of 2π.

SIMULATION ANALYSIS

In this section, the design approach of the elliptical quadrant radiator-based UWB antenna is discussed. The stepwise development of the proposed antenna is presented in Figure 5 after dividing it into four stages, i.e., Stage 1 to Stage 4. The corresponding simulated reflection coefficients are also depicted in Figure 5. The antenna optimization is performed to achieve a wide operational bandwidth ($|S_{11}|$<–10 dB) over the frequency span of 3.1–10.6 GHz. As a starting point, a traditional rectangular monopole antenna is perceived following the design procedure introduced in [32]. Rectangular printed monopole antennas are considered a promising candidate for UWB applications as they offer better design flexibility and higher miniaturization in comparison to other traditional printed geometries. The antenna structure is then chopped into two halves, keeping the full feeding line highlighted as in [23] to meet the miniaturization objective. These two steps, combined, are defined as Stage 1 of the design process. The corresponding antenna exerts an impedance bandwidth of ~59% (6.77–12.54 GHz).

An asymmetric feeding mechanism is adopted to widen the impedance bandwidth further and improve the resonance characteristics, which is now defined as Stage 2. The offset microstrip feed line enables the excitation of additional resonance and strong EM coupling between the radiator and the partial ground plane, providing broader impedance matching. The succeeding antenna design stage involves replacing the partial ground plane of Stage 2 with an expanded C-shaped ground plane in Stage 3. This modification further reduces the lower frequency and increases the operating bandwidth by providing a longer surface current path in the ground plane. The stated approach enhances the impedance matching with a bandwidth of 88%.

In the final stage (Stage 4), the reference radiator shape is altered to an elliptical quadrant shape geometry. The radiator allows some strong current density across the curved edge, which induces resonance characteristics near the lower end of the U.S. Federal Communications Commission-specified frequency range. As a result, the desired performance characteristic is successfully achieved, covering a wide impedance bandwidth of ~106% (3.13–11.74 GHz).

The next step is to investigate the role of the copper-coated dielectric reflector. As highlighted in the sub-section "UWB Antenna with Reflector," it is important to design and place the reflector material effectively such that the reradiated waves become in phase with the forward radiated waves. The reflector size and position optimization are performed by analyzing their effect on the antenna gain and bandwidth.

From the fundamental theories on reflector antennas, the suggested copper-coated dielectric reflector may be thought of as a specific example of a corner-reflector antenna with a corner

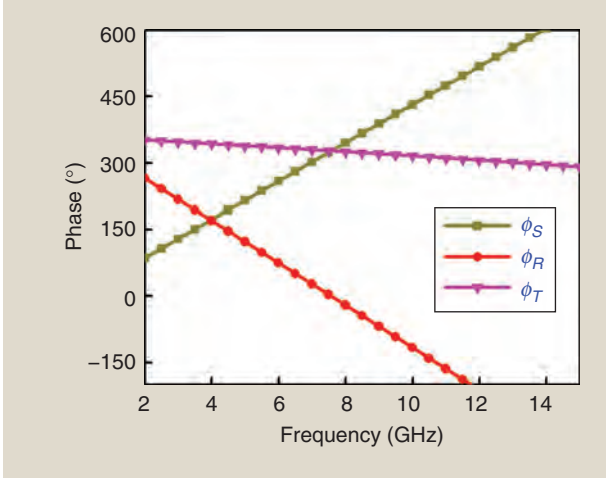

FIGURE 4. The predicted phase performance of ϕ_T, ϕ_R, and ϕ_S.

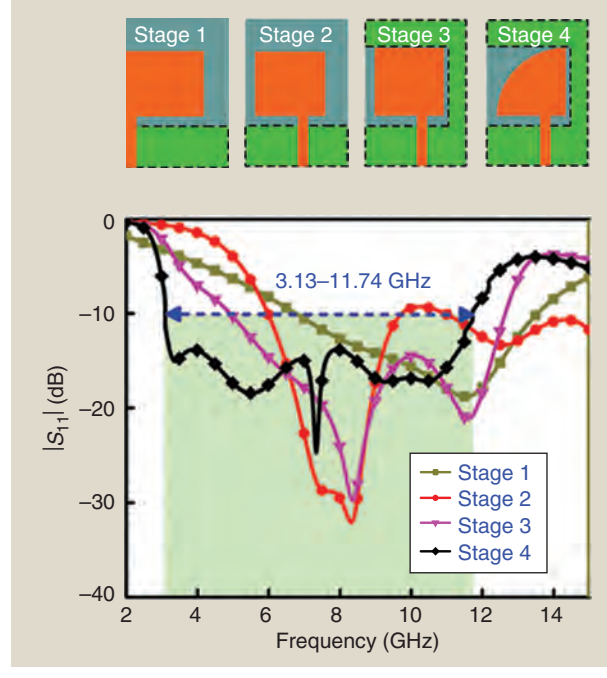

FIGURE 5. Reflection coefficients for the various stages of the antenna design.

angle of 180°. Now, it is also an established fact that the aperture size of a corner-reflector antenna should be kept between 1 and 2λ long to achieve an average gain boost of 7–8 dBi. Based on these principles, the authors conducted a parametric study starting with $X_r (= 11\ \text{mm})$ and $Y_r (= 18\ \text{mm})$, which are nearly half wavelength (20 mm) at the center operating frequency of 7.8 GHz. The length (Y_R) is varied between 18 mm to 48 mm, and the width (X_R) is varied between 11 mm and 41 mm, both with an incremental step of 10 mm. The reflection coefficient response curves indicate a negligible effect of the reflector size on the bandwidth and resonance characteristics [Figure 6(a)]. However, a significant variation in the gain characteristics of the antenna is noticed. Altering the reflector dimension ($X_R \times Y_R$) from 11×18 to $41 \times 48\ \text{mm}^2$ enhances the antenna maximum gain by approximately 70%, from 5.95 dBi to 10.14 dBi, as seen in Figure 6(b). A further increment in the dielectric reflector dimensions exerts a little improvement in the overall system gain. Therefore, the optimum dimensions are kept fixed at $X_R \times Y_R = 41 \times 48\ \text{mm}^2$.

The distance (S) contribution between the antenna ground plane and the dielectric reflector in enhancing the antenna performance is studied in the next step. The distance is varied from 6 to 24 mm, and the corresponding variations are displayed in Figure 7. It can be seen that proximity between the antenna and the reflector layer increases the capacitive coupling between the two elements, which disturbs the impedance matching of the antenna system [Figure 7(a)]. Further, an increase in S allows for more in-phase reflection of EM waves with the antenna's radiated forward waves, which develops stable gain characteristics over the desired wide frequency range [Figure 7(b)].

The influence of the dielectric slab reflector is analyzed further by taking the copper coating in four different ways: copper coating on top side, bottom side, both sides, and only with the dielectric reflector. The simulated gain for all of the cases is shown in Figure 8(a). It can be observed that the bottom-side copper-coated dielectric reflector is the best choice, with a maximum gain of 10.14 dBi. The gain is approximately 20% higher than that of the dielectric with

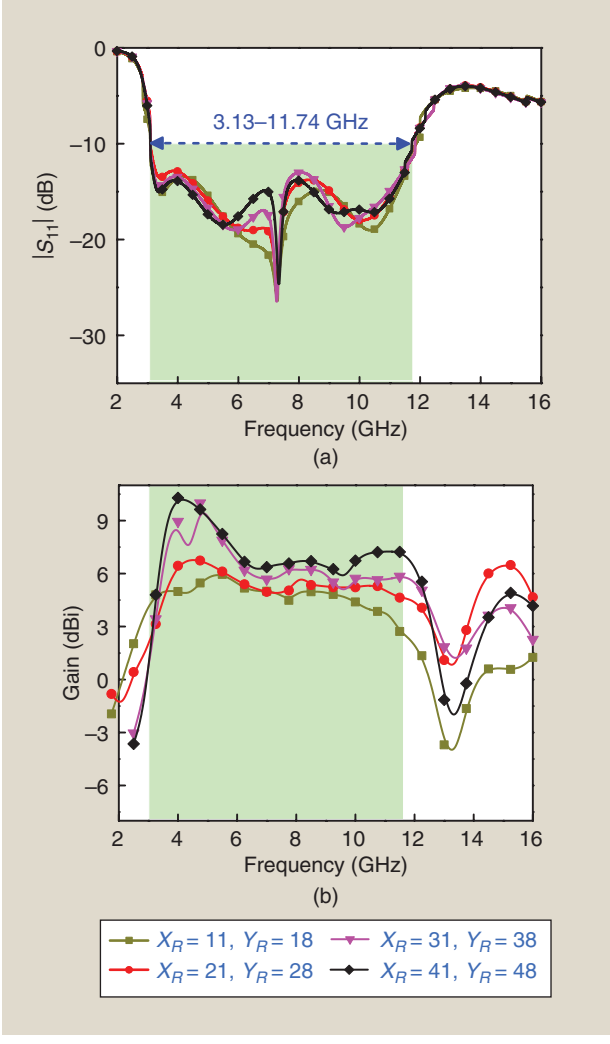

FIGURE 6. Effects of the reflector dimension on antenna performance: (a) reflection coefficients and (b) gain characteristics. X_R and Y_R values are in millimeters.

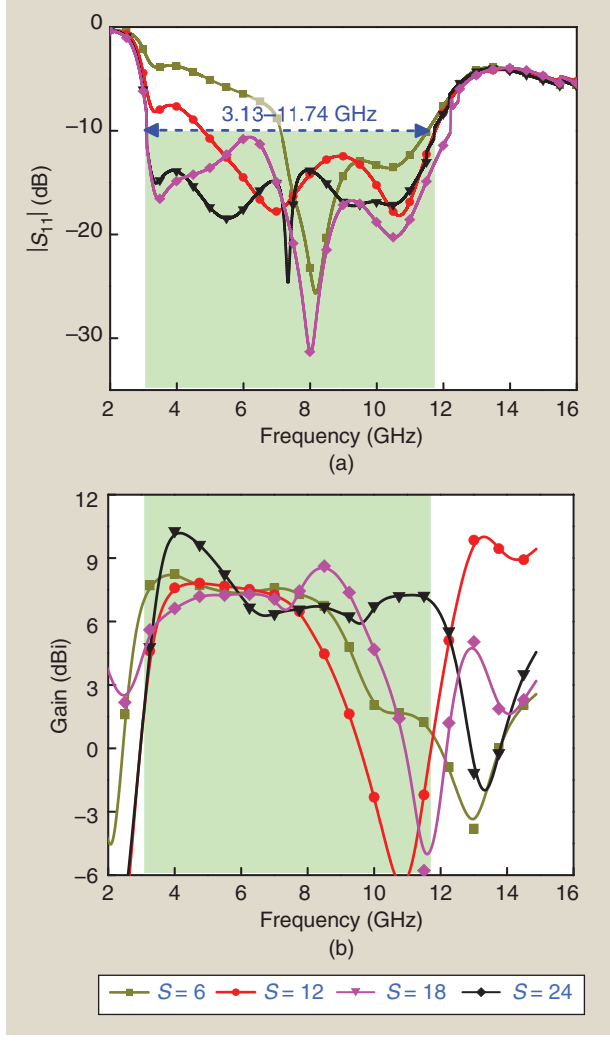

FIGURE 7. Effects of the reflector position on antenna performance: (a) reflection coefficient and (b) gain. Values of S are in millimeters.

top side (8.46 dBi) and both side metals (8.41 dBi) and 114% higher than the only-dielectric reflector (4.72 dBi). The maximum gain corresponding to the bottom-side copper-coated reflector can be attributed to the uniform phase variation characteristics obtained in the antenna plane, as discussed in the section "Theory of Reflector Plane in Gain Enhancement." The simulated antenna gain without the backside reflector is also obtained and presented in Figure 8(a) to illustrate the significant enhancement in the gain value from 2.91 dBi to higher values in all four cases. The front-to-back ratio (FBR) of the proposed antenna in the presence and absence of the reflector has also been determined and plotted in Figure 8(b). An average enhancement of 15 dB can be witnessed within the operating bandwidth of the reflector-backed UWB antenna.

To measure the influence of the designed reflector-loaded UWB antenna on the time domain, two identical antennas were used as the receiving and transmitting devices to construct the time-domain simulation scene. The distance between the two antennas is kept at 400 mm, which satisfies the far-field radiation conditions. The group delay variation against frequency, for both the face-to-face and side-by-side arrangements, is curved in Figure 9(a), displaying a uniform variation across the operating bandwidth. The uniform group delay variation ensures a distortionless pulse transmission from the antenna. Figure 9(b) shows the time-domain impulse response of the antenna with and without reflectors placed in parallel. The antennas with and without the reflector have very similar received signals, indicating no pulse distortion due to the reflector.

FABRICATION AND EXPERIMENTAL VALIDATION

To carry out the experimental validation, a prototype, shown in Figure 10(a), is fabricated. Polystyrene foam material ($\varepsilon_r \sim 1.1$) is used to fix the reflector at an appropriate distance from the antenna. The prototype is characterized using a vector network analyzer (VNA), and the radiation characteristics are determined using an anechoic chamber. Figure 10(b)

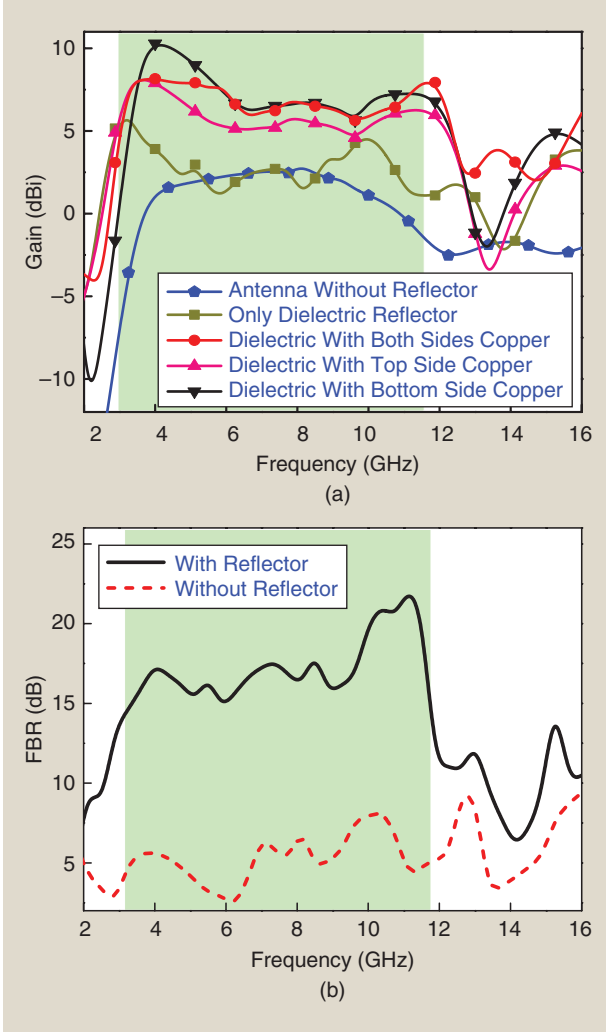

FIGURE 8. (a) The gain variation for different configurations of dielectric reflectors. (b) FBR with and without the dielectric reflector. FBR: front-to-back ratio.

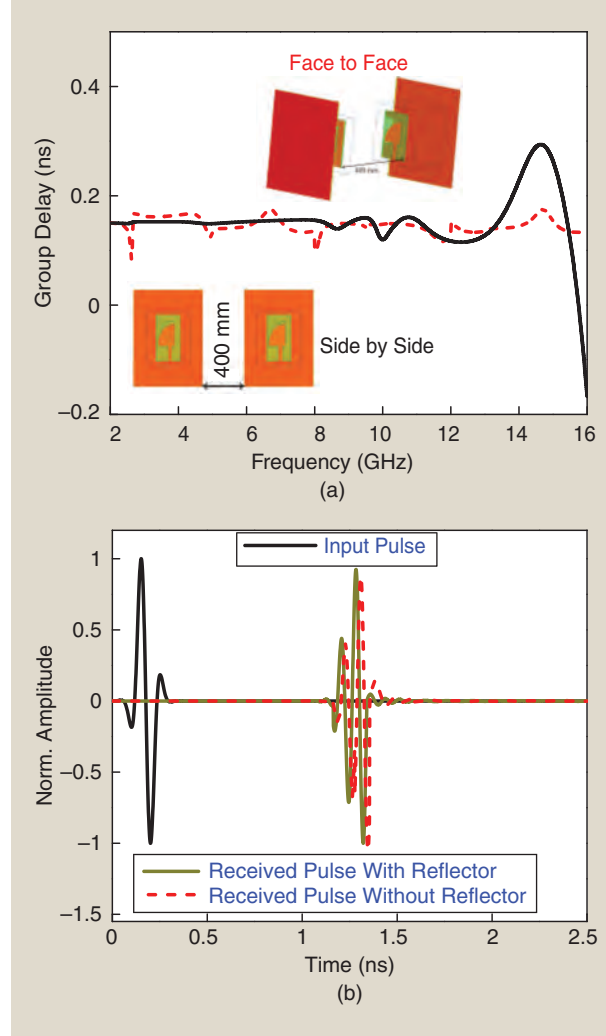

FIGURE 9. (a) The group delay variation in different orientations of the antenna. (b) The time-domain characterization in presence and absence of the reflector.

presents the simulated and measured reflection coefficients. The simulated bandwidth is 3.13–11.74 GHz, which almost coincides with the measured bandwidth of 3.19–11.83 GHz. A slight impedance mismatch is noted toward the higher frequencies, mainly due to the fabrication tolerance, soldering effect, foam support, and sub-miniature (SMA) coaxial cable connector losses. The measured gain variation values agree well with their simulated counterparts, with a maximum gain

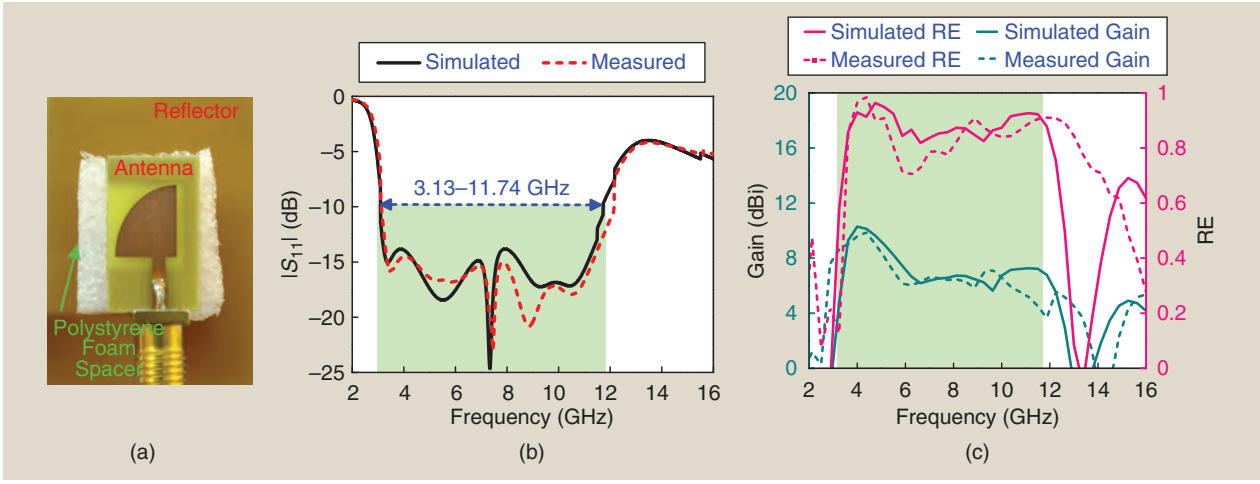

FIGURE 10. Experimental validation. (a) Fabricated prototype, (b) $|S_{11}|$, and (c) gain and RE characteristics. RE: radiation efficiency.

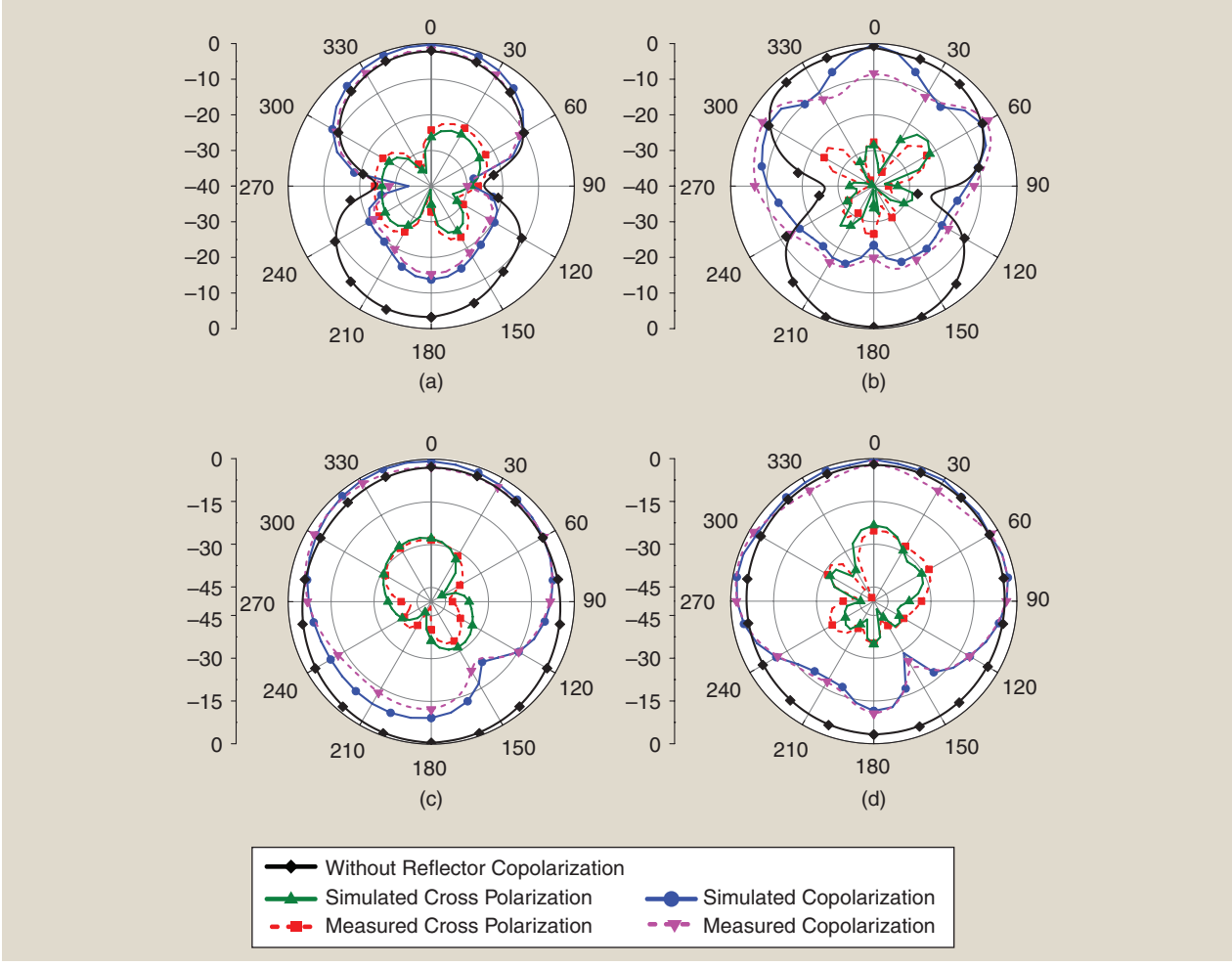

FIGURE 11. Far-field radiation patterns of the antenna with and without the reflector element. (a) E-plane, 4.5 GHz; (b) E-plane, 9.5 GHz; (c) H-plane, 4.5 GHz; and (d) H-plane, 9.5 GHz.

TABLE 2. A COMPARISON WITH THE EXISTING LITERATURE.

Reference	Gain-Enhancement Technique	Dimensions ($\lambda_g \times \lambda_g \times \lambda_g$)	f_c (GHz)	BW (GHz)	Peak Gain (dBi)
[7]	Vivaldi	$3.8 \times 5 \times 0.1$	1.2	0.3–2	11.5
[9]	Tapered slot	$3 \times 1.6 \times 0.1$	3.3	0.64–6	–
[11]	Bow-tie	$4.8 \times 4.8 \times 0.7$	3	0.42–5.5	7.96
[2]	Cavity backed	$0.6 \times 1.1 \times 0.1$	0.5	0.25–0.75	–
[17]	AMC	$1.8 \times 1.8 \times 0.9$	6.3	2.5–10	7.7
[18]	FSS 1	$3.5 \times 3.5 \times 0.9$	6.8	2.5–11	9
	FSS 2	$2.6 \times 2.6 \times 0.9$			8.5
[19]	FSS	$4.4 \times 4.4 \times 1.6$	7.5	3–12	8.9
[20]	FSS	$1.2 \times 1.2 \times 0.8$	8.2	3.1–13.4	8.5
[21]	FSS	$1.5 \times 1.5 \times 0.3$	7.5	3.05–11.9	7.9
This work	**Copper-coated dielectric reflector**	$\mathbf{1.1 \times 1.2 \times 0.5}$	**7.5**	**3.2–11.8**	**10**

λ_g: guided wavelength at f_c; f_c: center frequency; BW: relative bandwidth.

of 9.95 dBi, as shown in Figure 10(c). The average radiation efficiency (RE) also lies in the range of 75%–95%, in both the simulation and the measurements.

Finally, the radiation characteristics of the antenna in the two principal planes (E-plane and H-plane) are obtained and plotted in Figure 11. A slight disagreement is noted in the case of the measured results toward the higher frequencies, mainly due to the fabrication tolerance, soldering effect, foam support, and SMA connector losses. A comparison with the existing literature to highlight the advantages of the proposed high-gain UWB antenna system is presented in Table 2. It can be inferred that the proposed antenna, exhibiting a high-gain characteristic, is comparable with some of the contemporary GPR antenna systems. The reduction in circuit dimensions maintaining UWB is also quite prominent in the case of the proposed antenna. The proposed antenna system's lightweight characteristics qualify it for portable handheld wireless GPR systems.

EXPERIMENTAL TEST WITH SIMPLE SAND SYSTEM

To further validate the functional capability of the fabricated UWB antenna in GPR settings, experimental tests are conducted. The experimental setup for the test is adopted from the approach followed in [7] and [15]. Two identical copies of the proposed fabricated UWB antenna are placed on a wooden frame with a 40-cm (center-to-center) interval. One antenna is set to be the transmitting antenna, whereas the other is the receiving antenna. A metal sphere with a 5-cm diameter is buried 10 cm underground to serve as a subsurface target. The experimental results obtained from the VNA are processed through an inverse Fourier transform to collect the performance in the time domain, and the corresponding variation is shown in Figure 12(b). This image is a result of a B-scan with the clear presence of a hyperbolic curve near 6–10 ns, indicating the detection of a metal target by the GPR system. Reflections from the sand surface can also be witnessed clearly on the B-scans between 1 and 2 ns. The data considered in Figure 12(b) are just raw data that has been obtained only to testify the appropriateness of the proposed GPR antenna in real environments. These data require further application of signal and image processing methods to improve the resolution, which has not been considered as a part of this investigation.

CONCLUSIONS

The gain enhancement of a UWB antenna using a flat one-side copper-coated dielectric reflector has been investigated. A comprehensive analysis has been carried out to show the dielectric reflector's effects on bandwidth, gain, and directivity by considering the reflector length, width, and position. At an optimum air gap of 18 mm, the gain of the UWB antenna has

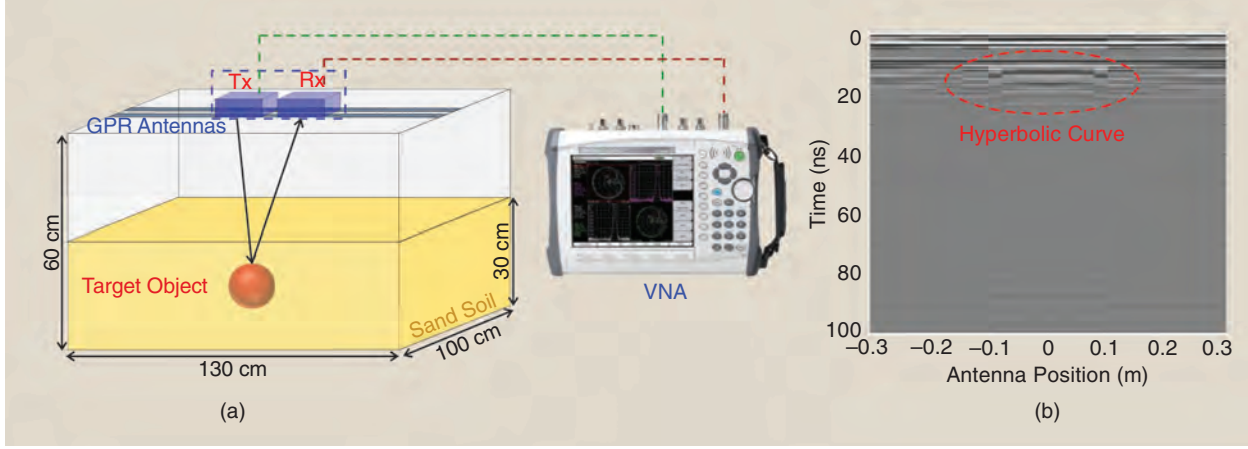

FIGURE 12. (a) A schematic representation of the GPR experimental setup. (b) A mapping of the B-scan results. Tx: transmitter; Rx: receiver.

been enhanced by approximately 7 dB. A wide bandwidth of 3.19–11.83 GHz and an improved peak gain of 9.95 dBi have been obtained with the optimized reflector-backed antenna, which is approximately 242% more than the standalone UWB antenna with a peak gain of 2.91 dBi. The measured results indicate the ability of the proposed UWB antenna for use in real-field high-gain GPR-sensing applications.

ACKNOWLEDGMENT

This work was supported by the Science and Engineering Research Board, Department of Science and Technology, Government of India under research Grant SB/S3/EECE/093/2016. Taimoor Khan is the corresponding author.

AUTHOR INFORMATION

Partha P. Shome (shomepartha16@gmail.com) is with the Department of Electronics and Communication Engineering, Dr. B R Ambedkar National Institute of Technology, Jalandhar 144011, India. He is a Member of IEEE.

Taimoor Khan (ktaimoor@ieee.org) is with the Department of Electronics and Communication Engineering, National Institute of Technology Silchar, Cachar 788010 India. He is a Senior Member of IEEE.

Binod K. Kanaujia (bkkanaujia@yahoo.co.in) is with the Department of Electronics and Communication Engineering, Dr. B R Ambedkar National Institute of Technology, Jalandhar 144011, India. He is a Senior Member of IEEE.

Ahmed A. Kishk (kishk@encs.concordia.ca) is with the Department of Electrical and Computer Engineering, Concordia University, Montreal, QC H3G 1M8, Canada. He is a Life Fellow of IEEE.

Yahia M. M. Antar (antar-y@rmc.ca) is with the Department of Electrical and Computer Engineering, Royal Military College of Canada, Kingston, ON k7k7b4, Canada. He is a Life Fellow of IEEE.

REFERENCES

[1] D. Daniels, *Ground Penetrating Radar*, 2nd ed. Piscataway, NJ, USA: IEEE Press, 2004.

[2] B. Wu, Y. Ji, and G. Fang, "Analysis of GPR UWB half-ellipse antennas with different heights of backed cavity above ground," *IEEE Antennas Wireless Propag. Lett.*, vol. 9, pp. 130–133, Mar. 2010, doi: 10.1109/LAWP.2010.2044475.

[3] J. Eilers, S. Anger, and T. Neff, "Radar based system for space situational awareness," *J. Space Orientations Communicator*, vol. 13, no. 4, pp. 1–13, 2016.

[4] B. Yektakhah, J. Chiu, F. Alsallum, and K. Sarabandi, "Low-profile, low-frequency, UWB antenna for imaging of deeply buried targets," *IEEE Geosci. Remote Sens. Lett.*, vol. 17, no. 7, pp. 1168–1172, Jul. 2020, doi: 10.1109/LGRS.2019.2942007.

[5] A. S. Turk and B. Sen, "Ultra-wide band antenna designs for ground penetrating impulse radar systems," in *Proc. IEEE Int. Symp. Electromagn. Compatibilities*, May 2003, vol. 2, pp. 888–891, doi: 10.1109/ICSMC2.2003.1429051.

[6] H.A. Mohamed, H. Elsadek, and E.A.F. Abdallah, "Design of compact DRH antenna for GPR transmitter application," in *Proc. 2nd Middle East Conf. Antennas Propag.*, Cairo, Egypt, 2012, pp. 1–4, doi: 10.1109/MECAP.2012.6618186.

[7] J. Guo, J. Tong, Q. Zhao, J. Jiao, J. Huo, and C. Ma, "An Ultrawideband antipodal Vivaldi antenna for airborne GPR application," *IEEE Geosci. Remote Sens. Lett.*, vol. 16, no. 10, pp. 1560–1564, Oct. 2019, doi: 10.1109/LGRS.2019.2905013.

[8] L. Guo, H. Yang, Q. Zhang, and M. Deng, "A compact antipodal tapered slot antenna with artificial material lens and reflector for GPR applications," *IEEE Access*, vol. 6, pp. 44,244–44,251, Aug. 2018, doi: 10.1109/ACCESS.2018.2864618.

[9] J. Shao, G. Fang, Y. Ji, K. Tan, and H. Yin, "A novel compact tapered-slot antenna for GPR applications," *IEEE Antennas Wireless Propag. Lett.*, vol. 12, pp. 972–975, Aug. 2013, doi: 10.1109/LAWP.2013.2276403.

[10] A. Raza, W. Lin, Y. Chen, Z. Yanting, H. T. Chattha, and A. B. Sharif, "Wideband tapered slot antenna for applications in ground penetrating radar," *Microw. Opt. Technol. Lett.*, vol. 62, no. 7, pp. 2562–2568, Feb. 2020, doi: 10.1002/mop.32338.

[11] K. K. Ajith and A. Bhattacharya, "A novel compact super-wideband bowtie antenna for 420 MHz to 5.5 GHz operation," *IEEE Trans. Antennas Propag.*, vol. 66, no. 8, pp. 3830–3836, Aug. 2018, doi: 10.1109/TAP.2018.2836382.

[12] M. S. Hendevari, A. Pourziad, and S. Nikmehr, "A novel ultra-wideband monopole antenna for ground penetrating radar application," *Microw. Opt. Technol. Lett.*, vol. 60, no. 9, pp. 2252–2256, Sep. 2018, doi: 10.1002/mop.31335.

[13] R. F. Harrington, *Field Computation by Moment Methods*. New York, NY, USA: Macmillan, 1968.

[14] J. V. Bladel, *Electromagnetic Fields*. New York, NY, USA: Hemishpere, 1985.

[15] M. Li, R. Birken, N. X. Sun, and M. L. Wang, "Compact slot antenna with low dispersion for ground penetrating radar application," *IEEE Antennas Wireless Propag. Lett.*, vol. 15, pp. 638–641, 2016, doi: 10.1109/LAWP.2015.2465854.

[16] Q. Rao, T. A. Denidni, and R. H. Johnston, "Dielectric reflector backed aperture-coupled antennas for reduced back radiation," *IEEE Trans. Electromagn. Compat.*, vol. 48, no. 2, pp. 287–291, May 2006, doi: 10.1109/TEMC.2006.874088.

[17] R. V. Dwivedi and U. K. Kommuri, "Compact high gain UWB antenna using fractal geometry and UWB-AMC," *Microw. Opt. Technol. Lett.*, vol. 61, no. 3, pp. 787–793, Mar. 2019, doi: 10.1002/mop.31602.

[18] Y. Yuan, X. Xi, and Y. Zhao, "Compact UWB FSS reflector for antenna gain enhancement," *IET Microw., Antennas Propag.*, vol. 13, no. 10, pp. 1749–1755, 2019, doi: 10.1049/iet-map.2019.0083.

[19] F. A. Tahir, T. Arshad, S. Ullah, and J. A. Flint, "A novel FSS for gain enhancement of printed antennas in UWB frequency spectrum," *Microw. Opt. Technol. Lett.*, vol. 59, no. 10, pp. 2698–2704, 2017, doi: 10.1002/mop.30789.

[20] S. Kundu, A. Chatterjee, S. K. Jana, and S. K. Parui, "A compact umbrella-shaped UWB antenna with gain augmentation using frequency selective surface," *Radioengineering*, vol. 27, no. 2, pp. 448–454, 2018, doi: 10.13164/re.2018.0448.

[21] A. J. A. A. Gburi, I. Ibrahim, M. Y. Zeain, and Z. Zakaria, "Compact size and high gain of CPW-fed UWB strawberry artistic shaped printed monopole antennas using FSS single layer reflector," *IEEE Access*, vol. 8, pp. 92,697–92,707, May 2020.

[22] Ansys HFSS v16.0. [Online]. Available: https://www.ansys.com/en-in/products/electronics/ansys-hfss

[23] A. T. Mobashsher and A. Abbosh, "Utilizing symmetry of planar ultra-wideband antennas for size reduction and enhanced performance," *IEEE Antennas Propag. Mag.*, vol. 57, no. 2, pp. 153–166, Apr. 2015, doi: 10.1109/MAP.2015.2414488.

[24] G. Gao, B. Hu, and J. Zhang, "Design of a miniaturization printed circular-slot UWB antenna by the half-cutting method," *IEEE Antennas Wireless Propag. Lett.*, vol. 12, pp. 567–570, Apr. 2013, doi: 10.1109/LAWP.2013.2259790.

[25] S. Doddipalli and A. Kothari, "Compact UWB antenna with integrated triple notch bands for WBAN applications," *IEEE Access*, vol. 7, pp. 183–190, Dec. 2018, doi: 10.1109/ACCESS.2018.2885248.

[26] A. Abbas, N. Hussain, J. Lee, S. G. Park, and N. Kim, "Triple rectangular notch UWB antenna using EBG and SRR," *IEEE Access*, vol. 9, pp. 2508–2515, Jan. 2021, doi: 10.1109/ACCESS.2020.3047401.

[27] Z. Lasemiimeni, Z. Atlasbaf, and N. Karbaschi, "Dual-functional ultrawideband antenna with high fidelity factor for body area networks and microwave imaging systems," *IEEE Access*, vol. 9, pp. 112,930–112,941, Aug. 2021, doi: 10.1109/ACCESS.2021.3104511.

[28] J. Nan, H. Xie, M. Gao, Y. Song, and W. Yang, "Design of UWB antenna based on improved deep belief network and extreme learning machine surrogate models," *IEEE Access*, vol. 9, pp. 126,541–126,549, Sep. 2021, doi: 10.1109/ACCESS.2021.3111902.

[29] J. Li, H. Chen, J. Wang, S. Li, X. Yin, and H. Zhao, "Ultra-wideband antipodal tapered slot antenna with reflectionless notched band," *IEEE Antennas Wireless Propag. Lett.*, vol. 21, no. 3, pp. 431–435, Mar. 2022, doi: 10.1109/LAWP.2021.3124333.

[30] S. K. K. Dash, T. Khan, B. K. Kanaujia, and Y. M. M. Antar, "Gain improvement of cylindrical dielectric resonator antenna using flat reflector plane: A new approach," *IET Microw., Antennas Propag.*, vol. 11, no. 11, pp. 1622–1628, Sep. 2017, doi: 10.1049/iet-map.2017.0284.

[31] D. M. Pozar, *Microwave Engineering*, 4th ed. Hoboken, NJ, USA: Wiley, 2018.

[32] K. P. Ray, "Design aspects of printed monopole antennas for ultra-wide band applications," *Int. J. Antennas Propag.*, vol. 2008, Apr. 2008, Art. no. 713858, doi: 10.1155/2008/713858.